Ultrasensitive detection of superoxide anion released from living cells using a porous Pt-Pd decorated enzymatic sensor

Xiang Zhu, Tingting Liu, Hongli Zhao, Libo Shi, Xiaoqing Li, Minbo Lan

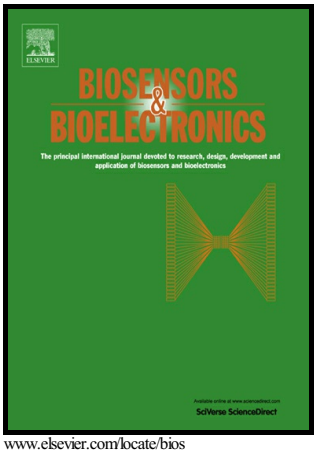

www.elsevier.com/locate/bios

PII: S0956-5663(15)30712-0
DOI: http://dx.doi.org/10.1016/j.bios.2015.12.061
Reference: BIOS8291

To appear in: *Biosensors and Bioelectronic*

Received date: 9 August 2015
Revised date: 18 December 2015
Accepted date: 19 December 2015

Cite this article as: Xiang Zhu, Tingting Liu, Hongli Zhao, Libo Shi, Xiaoqing L and Minbo Lan, Ultrasensitive detection of superoxide anion released from livin cells using a porous Pt-Pd decorated enzymatic sensor, *Biosensors an Bioelectronic,* http://dx.doi.org/10.1016/j.bios.2015.12.061

Ultrasensitive detection of superoxide anion released from living cells using a porous Pt-Pd decorated enzymatic sensor

Xiang Zhu[a], Tingting Liu[a], Hongli Zhao[a] *, Libo Shi[a], Xiaoqing Li[a], Minbo Lan[a, b] *

[a]Shanghai Key Laboratory of Functional Materials Chemistry, East China University of Science and Technology, Shanghai 200237, PR China

[b]State Key Laboratory of Bioreactor Engineering, East China University of Science and Technology, Shanghai 200237, PR China

* Corresponding authors. E-mails: minbolan@ecust.edu.cn; (M. B. Lan) honglizhao@ecust.edu.cn; (H. L. Zhao). Tel: +86-21-64253574, Fax: +86-21-64252947

Abstract: Considering the critical roles of superoxide anion ($O_2^{\bullet-}$) in pathological conditions, it is of great urgency to establish a reliable and durable approach for real-time determination of $O_2^{\bullet-}$. In this study, we propose a porous Pt-Pd decorated superoxide dismutase (SOD) sensor for qualitative and quantitative detection $O_2^{\bullet-}$. The developed biosensor exhibits a fast, selective and linear amperometric response upon $O_2^{\bullet-}$ in the concentration scope of 16 to 1536 μM (R^2 = 0.9941), with a detection limit of 0.13 μM (S/N = 3) and a low Michaelis-Menten constant of 1.37 μM which indicating a high enzymatic activity and affinity to $O_2^{\bullet-}$.

Inspiringly, the proposed sensor possesses an ultrahigh sensitivity of 1270 μA mM^{-1} cm^{-2}. In addition, SOD/porous Pt-Pd sensor exhibits excellent anti-interference property, reproducibility and long-term storage stability. Beyond our expectation, the trace level of $O_2^{\bullet-}$ released from living cells has also been successfully captured. These satisfactory results are mainly ascribed to (1) the porous interface with larger surface area and more active sites to provide a biocompatible environment for SOD (2) the specific biocatalysis of SOD towards $O_2^{\bullet-}$ and (3) porous Pt-Pd nanomaterials fastening the electron transfer. The superior electrochemical performance makes SOD/porous Pt-Pd sensor a promising candidate for monitoring the dynamic changes of $O_2^{\bullet-}$ *in vivo*.

Keywords: Porous Pt-Pd; Superoxide dismutase; Ultrahigh sensitivity; Superoxide anion detection; $O_2^{\bullet-}$ with Trace level; Living cells

1. Introduction

Up to date, remarkable interest has been paid to superoxide anion ($O_2^{\bullet-}$) for its critical roles in several pathological conditions including atherosclerosis, hypertension, diabetes, inflammation and postischemic myocardium (Valko et al. 2007). Besides, its function as second messengers to activate various signaling pathways also makes it a "star molecule" (Bézière et al. 2010). Therefore, the practical significance of monitoring $O_2^{\bullet-}$ in physiological environments has been well acknowledged in the past decade. Compared with electron spin resonance

(Abbas et al. 2014; Bézière et al. 2010), spectrophotometry (Hu et al. 2015; Robinson et al. 2006), chemiluminescence (Wang et al. 2014; Wardman 2007) and chromatography methods (Meany et al. 2007), electrochemical approach is more suitable for *in situ* and real-time analysis of $O_2^{\bullet-}$ due to its merits of low-cost instrumentation, facile operation and favorable performance (Kuila et al. 2011; Madhurantakam et al. 2014; Yuan et al. 2014). Recently, superoxide dismutase (SOD)-based sensors with high selectivity and sensitivity appear to be a hotspot for determining $O_2^{\bullet-}$ (Tang et al. 2015; Zhu et al. 2015). SOD can effectively catalyze the dismutation of $O_2^{\bullet-}$ to O_2 and H_2O_2 *via* a cyclic oxidation–reduction electron transfer mechanism. Unfortunately, the deeply buried redox centers of SOD results in the low electron transfer between SOD and electrode. In addition, lacking of an ideal interface for immobilization of SOD always makes sensors with poor reproducibility (Wang et al. 2012). In order to promote the electron transfer and reproducibility of prepared sensors, employing nanomaterials as carriers to immobilize enzyme is a feasible way.

Our group has utilized Pt-Pd alloys combination with carbon nanotubes as the support the immobilization of SOD for sensitive and selective $O_2^{\bullet-}$ detection (Zhu et al. 2015). In this work, SOD can efficiently catalyze the dismutation of $O_2^{\bullet-}$ to O_2 and H_2O_2 via a redox cycle of the copper complex moiety (Cu(I/II)) couple in Cu-Zn SOD (Di et al. 2015). Then,

the oxidation and reduction of H_2O_2 is effectively electrocatalyzed by Pt-Pd/MWCNTs. In order to further enhance the sensitivity of SOD sensors, one of the ideal ways is to promote the analytical performance of H_2O_2 originated from the dismutation reaction. Therefore, Pt-Pd alloys are still the promising candidate for fabrication $O_2^{\bullet-}$ sensors because the synergistic effect of Pt and Pd has great catalytic activities to enhance the performance of modified electrodes for H_2O_2 detection. (Sun et al. 2012)

Porous nanostructures with large electrochemical surface area, not only fasten the transport of electrolytes through the solid/liquid interface due to shortened diffusion length and beneficial diffusional regime, but also allow them to come into contact with more active surfaces through abundant pores and channels (Henstridge et al. 2010; Niu et al. 2013a). More importantly, the larger surface area is also perfect support for the immobilization of SOD and makes the redox centers of SOD has sufficient contact with $O_2^{\bullet-}$. (Jia et al. 2008; Jia et al. 2015; Lu et al. 2008; Trifonov et al. 2013; Yu et al. 2010; Zheng et al. 2014)

With the above concerns, we here recommend a fantastic electrochemical sensing interface assembled by a Pt-Pd porous structure for sensitive and selective $O_2^{\bullet-}$ determination. This interesting interface was originated from porous Cu foams formed by electrodeposition assisted with hydrogen evolution. We further decorated the porous Cu skeletons with Pt-Pd bimetal using a simple galvanic replacement process.

The porous structure was further used as support for SOD. To the best of our knowledge, there are no reports employing porous Pt-Pd materials as a biocompatible interface to immobilize SOD for $O_2^{\bullet-}$ detection. The electrochemical performances to $O_2^{\bullet-}$ were systematically studied using this proposed sensor. Moreover, the *in situ* monitoring of $O_2^{\bullet-}$ released from living cells is also investigated.

2. Experimental

2.1. Chemicals and apparatus

$CuSO_4$, H_2SO_4 and $H_2PtCl_6 \bullet 6H_2O$ were purchased from Sinopharm Chemical Reagent Co. and used directly without further purification. Anhydrous dimethyl sulfoxide, 18-crown-6, potassium dioxide (KO_2) and $(NH_2)PdCl_4$ were obtained from Aladdin Industrial Inc. D-glucose (Glu), L-ascorbic acid (AA), dopamine (DA), uric acid (UA), L-Glutathione reduced (GSH), 4-acetamidophenol (AP) and Zymosan A were commercially provided by Sigma-Aldrich. H_2O_2 was provided by Shanghai Lingfeng Chemical Reagent Co.. All analyte stock solutions were stored in 4 ^oC before utilization. Dulbecco's modified Eagle's medium (DMEM) cell culture medium, penicillin/streptomycin, trypsin and fetal bovine serum (FBS) were bought from Gibco Invitrogen. Hela cells derived from cervical cancer cells were purchased from Shanghai Institutes for Biological Sciences, Chinese Academy of Sciences. Ultrapure water (18.2 MΩ cm, Laboratory Water Purification Systems)

was used during all experiments. All other chemicals were of analytical grade and utilized as received.

The morphology of the as-synthesized Cu foam, porous Pt-Pd, dense Pt-Pd interface and porous Pt-Pd/SPCE with/without the immobilization of SOD was captured by scanning electron microscopy (SEM, JSM-6360LV, JEOL). The crystalline phase of the product was determined by X-ray diffraction (XRD, D/MAX-2550, Rigaku) with Cu Ka radiation (l = 0.15406 nm). The surface elemental composition was determined by X-ray photoelectron spectroscopy (XPS, ESCALAB 250Xi, Thermo Fisher) and energy dispersive spectroscopy (EDS, Falcon, EDAX).

2.2. Fabrication of porous Pt-Pd structure

The Pt-Pd porous structure was synthesized by two facile processes. **Step 1:** a porous Cu nanostructure was prepared *in situ* on a home-made screen-printed carbon electrodes (SPCE) substrate using the hydrogen evolution assisted electrodeposition strategy, which has been reported in our previous work (Niu et al. 2014). In a general process, SPCE was immersed into a precursor solution consisting of 0.2 M $CuSO_4$ and 1.0 M H_2SO_4 for 10 min allowing the precursor solution to contact with the substrate surface adequately; and then, an electrodeposition procedure with a constant current of -0.147 A (corresponding to a current density of approximately 3 A cm^{-2} if taking a geometric electrodeposition area of 0.049 cm^2 into account) was implemented for 30 s at room temperature.

The as-prepared Cu foam was rinsed with ultrapure water and dried in air. **Step 2:** porous Cu foam modified SPCE was dipped into an Ar saturated solution containing 25 mM $H_2PtCl_6 \cdot 6H_2O$ and 25 mM $(NH_2)PdCl_4$ for 2 h to accomplish the galvanic replacement. After reaction, the electrode was rinsed with ultrapure water carefully for further characterization and measurements. Finally, a selective electrochemical dealloying process was carried to selectively de-alloyed copper from the porous structure using CV methods scanning between -0.2 and 1 V in 0.05 M H_2SO_4 (An et al. 2015). In order to verify merits of Pt-Pd porous structure, a dense Pt-Pd material was also fabricated *via* the same procedures except the constant current was -0.005 A during the electrodeposition process.

2.3. Preparation of the SOD/Pt-Pd nanostructure electrodes

5 μL of SOD (3000 U/mL) and 2 μL of 0.05 wt% Nafion were drop-casted onto the prepared electrode surface of porous Pt-Pd/dense Pt-Pd interface, and dried at room temperature before use. The fabricated sensors were named as SOD/porous Pt-Pd/SPCE and SOD/dense Pt-Pd/SPCE.

2.4. Generation of superoxide anion

A stock solution of KO_2 was prepared by adding KO_2 to anhydrous dimethyl sulfoxide containing 18-crown-6, which can complex K^+ of KO_2 and increase the solubility of KO_2 in DMSO (Hyland and Auclair 1981). According to the molar absorptivity of $O_2^{\bullet-}$ in DMSO (2006 M^{-1} cm^{-1} at

271 nm), the concentration of $O_2^{\bullet-}$ could be estimated by UV-Vis spectroscope (Hyland and Auclair 1981; Luo et al. 2011) .

2.5. Electrochemical measurements

All amperometric measurements were performed on a CHI660D Electrochemical Analyzer (CH Instruments, China) with a conventional three-electrode system at room temperature. Unless otherwise states, all potentials reported here were referred to the saturated Ag/AgCl electrode. Cyclic voltammetric (CV) measurements were carried out in stationary electrolyte solutions. Chronoamperometric measurements were accomplished by injecting KO_2 into 5 mL 0.05 M PBS (pH 7.4) with the solution stirred constantly. Electrochemical impedance spectroscopy (EIS) test was carried out in 100 mM KCl solution containing 5 mM $Fe(CN)_6^{3-/4-}$ with frequency ranging from 100 kHz to 0.01 Hz. During experiment, PBS or DMEM cell culture medium containing 10% FBS and penicillin/streptomycin (1%) were all injected in a beaker. In order to remove O_2, we bubbled Ar gas into beaker containing solution for 10 min and uncovered this beaker to reduce the influence of O_2.

2.6. Cell Culture and Detection of Extracellular Release of $O_2^{\bullet-}$ released from cells

Hela cells were cultivated at 37 °C in 5% CO_2 in cell flasks containing DMEM with 10% FBS and 1% antibiotics. After the growth to 90% confluence, they were centrifugation and wash with PBS, and their

number were estimated by a hemocytometer to be 5×10^6. To detect the secretion of $O_2^{\bullet-}$ by living cells, Hela was first dispersed in 5 mL PBS. Then, 20 μL of Zymosan A (5 mg/mL) was injected into the above PBS solution and the amperometric current responses at the applied potential of -0.1 V were recorded. For comparison, the response of cells without addition of Zymosan A and testing system without cells acted as control groups.

3. Results and discussion

3.1. Characterization of the porous Pt-Pd interface

A facile electrodeposition assisted with hydrogen evolution method followed by a galvanic process was introduced to prepare this fascinate porous Pt-Pd interface. During the electrodeposition process, vigorous H_2 bubbles, generated from the reduction of H^+ to H_2 (Plowman et al. 2015), can be used as a dynamic template for Cu^{2+} ions electro-reduction to porous Cu foams. As depicted in Fig. S1(A), the phase characteristics of the Cu foam were identified from its XRD pattern. The remarkable peaks locate at 43.3^o, 50.4^o and 74.1^o are ascribed to the (110), (200) and (220) crystal planes of monoclinic Cu (JCPDS no.04-0836) (Niu et al. 2014). It is worth noting that another peaks position at 36.5^o and 61.5^o are ascribed to the (111) and (220) crystal planes of Cu_2O (JCPDS no.65-3288), which is the partial oxidation of nanostructured Cu exposed to air (Gao et al. 2015). The surface morphology of the Cu foams was observed by SEM.

As shown in Fig. S1(B), the porous Cu foams is a highly dendritic material and the underlying pores decreases along with the shorter distance away from substrate. Galvanic replacement has led to the fabrication of several nanostructured materials. As the substrate is a sacrificial template, the replaced structure may closely resemble the template on the macroscale (Plowman et al. 2015). After galvanic replacement reaction, the XRD pattern notably changes as shown in Fig 1(A). Owing to the fact that Pt and Pd share almost the same crystal structure, the difference of the XRD peak positions of Pt and Pd is not distinct. The representative diffraction peaks at 40°, 46°, 67° and 82° are attributed to the (111), (200), (220) and (311) planes of Pt-Pd with the face-centred cubic (FCC) structure. The position of peaks exist a slightly positive shift which indicating the formation of Pt-Pd alloy (Li et al. 2014). Fig 1(B) illustrates the surface morphology of porous Pt-Pd foam which has the similar macroscale structure of Cu foam. However, the dendritic structure of Cu foam becomes passivated which is also a proof of the formation of Pt-Pd alloy. For comparison, Pt-Pd material with a dense structure is prepared. Due to the relatively low constant current (-0.005 A), honeycomb liked structure can't be observed and some irregular particles appears (shown in Fig. S3(A)).

(Please insert **Figure 1** here)

The formation and the surface composition of porous Pt-Pd

nanostructure were further characterized by XPS technology. As depicted in Fig. 1(C), the peaks located at 69.5, 72.8, 333.5 and 339.5eV are ascribed to $Pt4f_{7/2}$, $Pt4f_{5/2}$, $Pd3d_{5/2}$ and $Pd3d_{3/2}$, respectively (Fig. S2), indicating the coexistance of Pt(0) and Pd(0). And the atom ratio of Pt and Pd is approximately 1:1 according to the table of elemental component (Fu et al. 2013). Without expectation, there is still a little Cu atom exists in microstructure. Peak position at 934.5 and 954.2 eV are assigned to Cu $2p_{3/2}$ and Cu $2p_{1/2}$ peaks and the Cu atom content is about 2.9% (Gao et al. 2015). The remaining Cu in the skeleton of porous structure prevents the bulk honeycomb structure from collapse. Similar results can be obtained from dense Pt-Pd materials. Cu, Pt and Pd atoms co-exist in the dense structure with the atom ratio of Pt, Pd and Cu of 14.04%：16.07%：4.8% (as shown in Fig. S3(B-E)). XPS results demonstrate porous and dense structure Pt-Pd materials have the similar atom composition.

The quantitative atom ration was characterized by EDS spectroscopy. The associated EDS pattern in Fig 1(D) verifies simultaneous existence of Pt and Pd in porous Pt-Pd NSs. Atom contents for Pt: Pd: Cu are 13.8%:17.2%:7.2% which fits well with XPS results. For comparison, Atom contents for Pt: Pd: Cu in dense structure are 14.4%:17.7%:4.9% which is similar to the data of porous Pt-Pd (shown in Fig. S3(F)).

The scheme of preparation process is described in supporting

information.

3.2. Electrochemical characteristics of the porous SOD/porous Pt-Pd electrode

Before the discussion of the electrochemical behavior of the proposal electrode, SEM and EIS methods were introduced to characterize the morphology of SOD sensor. As shown in Fig. S4, the surface of honeycomb structured porous Pt-Pd looks rough and covers with some agglomerates. Agglomerates are obvious to be observed, indicating the existence of SOD, and the successful fabrication of enzyme electrode (Zhu et al. 2015). EIS is carried out to identify the change of the charge transfer resistance and/or capacitance on the electrode surface and further improve the immobilization of SOD. The EIS curves of porous/Pt-Pd/SPCE and SOD/Pt-Pd/SPCE are shown in Fig. S4(C). The charge transfer resistance (R_{ct}) of porous/Pt-Pd/SPCE is 236 Ω. After the modification of SOD on the electrode, the R_{ct} shows a slight increase to 402 Ω, indicating that the insulating effect occurs when SOD is immobilized on the electrode and increases the charge transfer resistance. This result is in accordance with our previous works and other studies. (Emregul et al. 2013; Singh et al. 2014; Tang et al. 2015; Wang et al. 2013; Zhu et al. 2015).

(Please insert **Figure 2** here)

Fig. 2(A) depicts CV curves of the fabricated electrodes in 0.1 M

deoxygenated H_2SO_4 recorded at a scan rate of 50 mV/s. The potential ranging from -0.1–0.1 V (versus Ag/AgCl) is identified to hydrogen adsorption/desorption. The potential regions from 0.6–0.9 V and 0.3–0.6 V are associated with anodic peak and cathodic peak of the Pt-Pd nanomaterial, respectively (Kuai et al. 2012; Zhang et al. 2012). By integrating the charge associated with this peak in H_2SO_4 medium with the Pt loading, the electrochemically active surface area (ECSA) of Pt-based material can be determined (Ding et al. 2012). Although Pt-Pd/SPCE is covered by SOD, the CV curves still maintain the characteristic of Pt based sensors. Therefore, we want to utilize this characteristic to calculate the ECSA of two kinds of sensors so as to further prove the superior of porous based sensors. Taking into account the Pt loading for porous Pt-Pd (12.6 μg) and dense Pt-Pd (13.5 μg) by using ICP-OES, ECSA for SOD/porous Pt-Pd/SPCE (30 m^{-2} g^{-1}) is 4 times higher than that for SOD/dense Pt-Pd/SPCE (7.5 m^{-2} g^{-1}), suggesting that more active sites are available for porous Pt-Pd material in comparison with the dense one.

EIS measurement is a useful tool to characterize the electron transfer ability. As can be seen from Fig. 2(B), SOD/porous Pt-Pd/SPCE exhibit good electron transfer power, the charge transfer resistance (R_{ct}) of 402 Ω is much smaller than R_{ct} of SOD/dense Pt-Pd/SPCE (850 Ω) and SOD/SPCE (8000 Ω). Owing to the large surface area and abundant

active sites, SOD/porous Pt-Pd/SPCE permits the increase electrical contact between the electrode and the redox label in solution, resulting in improved diffusion of ferricyanide molecules towards the electrode surface (Singh et al. 2014). The similar conclusion can be obtained from the typical CVs of three electrodes in 0.05 M PBS containing 5 mM $Fe(CN)_6^{3-/4-}$ at a scan rate of 20 mV s^{-1} in the potential range of -0.1 V to 0.5 V as shown in Fig. S5.

3.3. Electrochemical performance of SOD/Pt-Pd electrodes towards $O_2^{\bullet-}$

The Electrochemical behavior of enzymatic sensors towards $O_2^{\bullet-}$ was first evaluated by CV technology in the presence/absence of $O_2^{\bullet-}$. A typical Pt-based CV curve is displayed in Fig. 3. With regard to SOD/porous Pt-Pd/SPCE, remarkable signals of the reduction current appearing at 0.55 V is ascribed to the electro-reduction of Pt/Pd (Niu et al. 2013b). When different volumes of KO_2 are added, both the oxidation at 0.5 V and reduction currents at 0 V of SOD/porous Pt-Pd sensor gradually increases, indicating that this sensor has excellent response towards $O_2^{\bullet-}$ and the results are fit well with the previous report (Deng et al. 2008b; Ohsaka et al. 2002, ; Tang et al. 2015; Wang et al. 2012 ; Zhu et al. 2015). Similar phenomenon also occurs on SOD/dense Pt-Pd sensor. However, upon addition the same concentration of $O_2^{\bullet-}$, the current response for sensor with dense structure is much smaller than that with

porous one, which indicates SOD/porous Pt-Pd/SPCE has better electrochemical property towards $O_2^{\bullet-}$.

(Please insert **Figure 3** here)

We here arises a serious question: whether the current signal we detect is ascribed to $O_2^{\bullet-}$. To answer this question, a typical amperometric response of SOD/porous Pt-Pd/SPCE toward $O_2^{\bullet-}$ was carried out at -0.1 V. As shown in Fig. S6, after injection KO_2 into the solution to generate $O_2^{\bullet-}$, a fast and obvious signal response is obtained. Surprisingly, with the addition of SOD, which is also a selective scavenger of $O_2^{\bullet-}$, the enhanced cathodic current decreases by > 98%. Therefore, the observed large cathodic current derives from $O_2^{\bullet-}$.

Fig. S7 compares the current changes of SOD/porous Pt-Pd/SPCE and SOD/dense Pt-Pd/SPCE upon addition of $O_2^{\bullet-}$ into phosphate buffer solution (PBS, pH 7.4) at -0.1 V vs. Ag/AgCl. Obviously, two sensors exhibit an increase of the amperometric responses at different degrees Considering the steady responses, the SOD/porous Pt-Pd/SPCE offers a current change of 50 μA cm^{-2} for 0.12 mM $O_2^{\bullet-}$, while SOD/dense Pt-Pd/SPCE provide 20 μA cm^{-2}. Since the $O_2^{\bullet-}$ kinetics has been greatly dominated by the electrocatalytic rate of SOD based sensor, the catalytic rate constant (k_{cat}) can be calculated based on (Niu et al. 2013a):

$$\frac{I_{cat}}{I_L} = \pi^{1/2}(k_{cat}C_0t)^{1/2}$$

where C_0 is the bulk concentration of $O_2^{\bullet-}$, t is the elapsed time, and I_{cat} and I_L are the currents in the presence and absence of $O_2^{\bullet-}$, respectively. According to the slope of I_{cat}/I_L versus $t^{1/2}$, the k_{cat} of SOD/porous Pt-Pd/SPCE taking the $O_2^{\bullet-}$ concentration C_0 = 0.12 mM into account is 2 times higher than that of SOD/dense Pt-Pd supported SPCE. This result matches well with the CV curve of two sensors towards the detection of $O_2^{\bullet-}$ above and indicates sensor with porous structure has superior electrochemical performance towards $O_2^{\bullet-}$.

3.4. Amperometric detection of $O_2^{\bullet-}$

Prior to amperometric sensing of $O_2^{\bullet-}$, several parameters including the applied potential and pH value should be optimized. Firstly, the applied potential, which can strongly affect the detection, was evaluated by collecting the typical chronoamperometric responses of the proposed sensor towards $O_2^{\bullet-}$ at different applied potentials. It is obvious that sensor provides the maximum response at -0.1 V (as shown in Fig S8(A)). Therefore, an applied potential of -0.1 V vs. Ag/AgCl is selected as the optimized potential.

pH value of test environment which will affect the activity of SOD should also be studied. The effect of pH, ranging from 6.8 to 8.6, on the electrochemical behavior of proposed sensor was measured by CV technique in 0.05 M PBS containing 5 mM $Fe(CN)_6^{3-/4-}$ and 0.1 M KCl. The influence of pH studied in the presence of $Fe(CN)_6^{3-/4-}$ has a main

advantage. The obtained CV curves usually have a pair of nice reversible redox peaks, which will make it easy to research the relationship between redox peaks and electrochemical index. Although Pt-based materials have their unique CV curves, the oxidation peaks are sometimes hard to identify. So does the reduction peaks when the content of Pt is low. In order to precisely study the electrochemical behavior, the $Fe(CN)_6^{3-/4-}$ probe was employed. As shown in Fig. S8(B), SOD retains the highest enzymatic activity when the pH value is around the physical condition. Further experiments will select pH 7.4 as the optimum pH.

As displayed in Fig. S8(C), the loading of SOD was optimized by immobilization different amounts of SOD (1~6 μL) on the modified electrode. The optimum amount of enzyme used for immobilization onto the electrode surface is 3 μL due to the larger current response than those of other loading amounts. The smaller amount of enzyme (when the amount of enzyme is lower than 3 μL) gives lower sensitivity due to decreased loading of SOD. However, when the amount of the enzymes is too large (higher than 3 μL), the electrode shows very high electrochemical impedance due to that SOD can act as a resistance material, resulting in decreased sensitivity.

To get more reliable results, some other factors such as oxygen deficiency, the presence of chlorides ions and 18-crown-6 were also studied. As depicted in Fig. S9(A,B), it is observed that the response of

the electrode in air saturated solution is lower than that of the Ar saturated electrolyte. Therefore, the solution should bubble Ar gas for 10 min to eliminate the dissolved oxygen prior to analysis. Besides, Cl^- seems to show insignificant affection to $O_2^{\bullet-}$ detection due to the excellent poison resistance/anti-interference behavior of the sensor. 18-crown-6 is a co-solvent for increasing the solubility of KO_2. Therefore, we don't expect it will disturb the sensing of $O_2^{\bullet-}$. Fortunately, this species produces will not interfere the detection (as shown in Fig. S9(C)).

(Please insert **Figure 4** here)

With the above consideration, amperometric responses upon successive addition of $O_2^{\bullet-}$ into constantly stirred 0.05 M PBS (pH 7.4,) at the applied potential of -0.1 V were recorded. As depicted in Figure 5, well-defined amperometric currents increasing stepwise with the level of $O_2^{\bullet-}$ are obtained, with a response time of 3 s, indicating fast electro-transfer between interface and $O_2^{\bullet-}$. It is found that the current responses are linear with the $O_2^{\bullet-}$ concentrations from 16 to 1536 μM (Figure 7B), with a correlation coefficient of 0.9941 (n = 5). The limit of detection (LOD) is calculated to be as low as 0.13 μM, based on the signal/noise value of 3 (S/N = 3). The sensitivity of the prepared sensor is 1270 μA mM^{-1} cm^{-2}. It is worth mentioning that in comparison with other sensors based on SOD for $O_2^{\bullet-}$ detection, our proposed sensor provides higher sensitivity and wider linear range (as list in Table 1).

(Please insert **Table 1** here)

As enzymatic sensor, the apparent Michaelis-Menten constant (K_m^{app}), which is generally used to evaluate the affinity of an enzyme to its substrate, is also determined in the present work. The K_m^{app} can be estimated from the Linweaver-Burk equation (Kamin and Wilson 1980):

$$\frac{1}{i_{ss}} = \frac{1}{i_{max}} + \frac{K_m^{app}}{i_{max}} \times \frac{1}{C}$$

where i_{ss} is the steady-state current, i_{max} is the maximum current, and *C* is the concentration of $O_2^{\bullet-}$. It is calculated that the K_m^{app} value for SOD/porous Pt-Pd/SPCE is 1.37 μM. The low value of K_m^{app} indicates that SOD modified porous Pt-Pd interface has a high enzymatic activity and affinity to $O_2^{\bullet-}$.

Selectivity of detection is an important factor for a reliable sensor. In the present study we discussed the effects of common possible interfering species such as AA, DA, UA, AP, GSH and Glu on the selective monitoring of $O_2^{\bullet-}$. In addition, H_2O_2 is one of the main by-products in the enzyme-catalytic system, therefore, the specificity of the sensor against H_2O_2 is of great importance in its application for the determination of $O_2^{\bullet-}$. As displayed in Fig. S10(A), the typical chronoamperometric responses upon successive addition of 0.08 mM $O_2^{\bullet-}$, 0.5 mM H_2O_2, Glu, GSH, AA, UA, AP and DA 0.05 M PBS (pH 7.4) are recorded. For a better comparison, we set the current intensity of 0.08

mM $O_2^{\bullet-}$ as 100%, and the other electrochemical responses are normalized by this value. AA, DA, UA, AP, GSH and Glu produce no notable current responses interfering the detection because these species cannot be electrochemically oxidized at this relatively low potential (-0.1 V). To our great surprise, the current intensity of H_2O_2 is only 5% compared to $O_2^{\bullet-}$ (100%). The possible reason may be: (1) although Pt-Pd alloy has superior ability to catalyze the reduction of H_2O_2, the surface of porous Pt-Pd is covered with a layer of SOD (as shown in SEM figure), which has a high selectivity towards $O_2^{\bullet-}$. Therefore, exogenous H_2O_2 can be effectively disturbed. (2) the outermost Nafion layer as an effectively pre-selective barrier also can reduce the interference from exogenous H_2O_2.

The fabrication reproducibility of eight newly-prepared showed an acceptable reproducibility with a RSD of 2.4% for the current response of 0.08 mM $O_2^{\bullet-}$. Moreover, the long-term stability is also evaluated by collecting amperometric responses of 0.08 mM $O_2^{\bullet-}$ every two days for 31 days (As displayed in Fig. S10(B)). After one month, the biosensors still maintain a high sensitivity for $O_2^{\bullet-}$ detection compared to the initial one. On the one hand, the Nafion layer prevents materials on the electrode surface from leakage when testing. On the other hand, the good durability and biocompatibility of porous Pt-Pd interface provides a perfect microenvironment for SOD to retain its bioactivity.

3.5. Mechanism of $O_2^{\bullet-}$ sensing

We have refer in introduction that our previous sensor followed the mechanism that SOD catalyzes the dismutation of $O_2^{\bullet-}$ to O_2 and H_2O_2 and then the oxidation and reduction of H_2O_2 is electrocatalyzed by Pt-Pd/MWCNTs. However, in this work, we have find out the detection of $O_2^{\bullet-}$ of SOD/porous Pt-Pd SPCE undergoes the mechanism of the direct electron transfer (DET) between copper, zinc-superoxide dismutase (Cu, Zn-SOD) and electrode. In the anodic process, SOD(oxidation form) oxidizes one $O_2^{\bullet-}$ to molecular oxygen, and itself is reduced to SOD(reduction form). In a reversal scan, the redox reaction between the SOD(reduction form) and another $O_2^{\bullet-}$ undergoes to produce SOD(oxidation form) and H_2O_2 (as shown in Fig. S11). The main evidence is that the proposed sensor can effectively exclude the interference from H_2O_2. If the detection of $O_2^{\bullet-}$ is based on the former mechanism, the interference of H_2O_2 can't be avoided. The reason is that: The redox center of SOD on a porous is more sufficient to expose and electron transfer in porous Pt-Pd structure is much easier than that in our previous Pt-Pd-MWCNTs structure (as shown in Fig. S12). Therefore, the porous structure makes DET between SOD and electrode come true. Unfortunately, a pair of redox peaks of SOD wasn't obviously observed. A possible reason is that the bulk current of porous material is too large to overlap the redox peaks, therefore, only the typical characteristic can be

obtained (as shown in Fig. S13). This phenomenon also happens when employing other porous structure zeolite to immobilize enzyme. (Jia et al. 2015; Ren et al. 2013; Trifonov et al. 2013).

3.6. Real sample analysis

In order to test properties of the proposed sensors in sophisticated system, real sample analysis was performed in DMEM cell culture medium containing 10% FBS, and penicillin/streptomycin (1%) using a calibration curve method to determine the recoveries of various concentration of $O_2^{\bullet-}$. As described in our previous work, the sample was prepared by spiking different concentration of $O_2^{\bullet-}$ into the mixture of 4 mL PBS and 1 mL DMEM cell culture medium and the final concentration of $O_2^{\bullet-}$ was 0 (as control group), 40, 80, 120 μM, respectively. The recovery is 96.2%, 98.5% and 98.6% with R.S.D. of 2.8%, 1.9% and 2.3%**.** The results (as shown in table S1) demonstrate that sensors are suitable for usage in a sophisticated environment.

3.7. Detection of Extracellular Release of $O_2^{\bullet-}$ released from Hela cells

Recovery test has improved that our sensor possesses the ability of reliable detection of $O_2^{\bullet-}$. In this part, we further utilized the proposed sensor to detect of $O_2^{\bullet-}$ released from living Cells. Zymosan can induce inflammation responses include the induction of proinflammatory cytokines, arachidonate mobilization, protein phosphorylation, and inositol phosphate formation, which can stimulate superoxide production

in living cells. (Assreuy et al. 1994; Dimitrova et al. 2010; Lin et al. 2008; Wu et al. 2011;). Curve a in Fig. 5 depicts electrochemical responses obtained at SOD/Porous Pt-Pd/SPCE in PBS (pH = 7.4) without Hela cells, after addition of Zymosan A, no notable change of the amperometric responses is observed which indicate that Zymosan A scarcely influence the extracellular $O_2^{\bullet-}$ detection. Curve b and c in Fig. show the amperometric response changes of sensor located at the living cell suspension. After injecting 20 μL of Zymosan A (5 mg/mL) into the solution, a significant increased current is observed (curve c), followed by a gradual decrease of current, which means the Zymosan A induced extracellular $O_2^{\bullet-}$ release is a transient process. However, the control well containing no Zymosan A doesn't generate any signal response. Curve a was conducted in pure PBS solution without addition of cells. PBS solution is a homogeneous solution without suspended substance. When conducted the experiment, PBS curve would not cause obvious perturbation in baseline. However, the curve b and c was performed in a cell suspension and during the stirring process, cell would contact with the surface of electrode and caused some noise in baseline. In a brief summary, we considered the noise level in curve b and c are originated from the perturbation of suspension cell to the electrode. The satisfactory result is ascribed to the sensitivity, selectivity and reliability of fabricated sensors for intracellular $O_2^{\bullet-}$ detection.

(Please insert **Figure 5** here)

4. Conclusions

In this work, a fascinating $O_2^{\bullet-}$ sensor have been successfully fabricated by employing a porous Pt-Pd honeycomb structure with large surface area, plenty of active sites and good biocompatibility for the immobilization of SOD. The proposed sensor can selectively, sensitively and reliably detect the $O_2^{\bullet-}$ in complicated biological system. Inspiringly, the trace level of $O_2^{\bullet-}$ released from Hela cells has been successfully captured using this sensor, indicating that the proposed electrode may have potential applications for *in vivo* monitoring the trace $O_2^{\bullet-}$.

Acknowledgements

This research was financially supported by National Natural Science Foundation of China (NSFC, no. 21305044) and Science and Technology Commission of Shanghai Municipality (STCSM, no. 13510710900).

References

Abbas, K., Hardy, M., Poulhès, F., Karoui, H., Tordo, P., Ouari, O., Peyrot, F., 2014. Free Radical Bio. Med. 71, 281-290.

An, C.Y., Zhuo, K., Kim, W.J., Chung, C.H., 2015. Sensor Actuat. B-Chem. 213, 329-333.

Assreuy, J., Cunhaoo, F.Q., Epperlein, M., Dutra, A., O'Donnellnm, C.A., Liewn, F.Y., Moncada, S.,1994. Eur. J. Immunol. 24, 672-676.

Bézière, N., Frapart, Y., Rockenbauer, A., Boucher, J.L., Mansuy, D., Peyrot, F., 2010. Free Radical Bio. Med. 49, 437-446.

Deng, Z.F., Rui, Q., Yin, X., Liu, H.Q., Tian, Y., 2008a. Anal. Chem. 80, 5839-5846.

Deng, Z.F., Tian, Y., Yin, X., Rui, Q., Liu, H.Q., Luo, Y.P., 2008b. Electrochem. commun. 10, 818-820.

Di, J., Bi, S., Zhang, M., 2004. Biosens. Bioelectron. 19, 1479-1486.

Dimitrova, P., Ivanovska, N., Schwaeble, W., Gyurkovska, V., Stover, C., 2010, Mol. Immuno. 47, 1458-1466.

Ding, L.X., Li, G.R., Wang, Z.L., Liu, Z.Q., Liu, H., Tong, Y.X., 2012. Chem. Eur. J. 18, 8386-8391.

Emregül, E., 2005. Anal. Bioanal. Chem. 383, 947-954.

Emregul, E., Kocabay, O., Derkus, B., Yumak, T., Emregul, K.C., Sınag, A., Polat, K., 2013. Bioelectrochemistry 90, 8-17.

Fu, G.T., Wu, K., Lin, J., Tang, Y.W., Chen, Y., Zhou, Y.M., Lu, T.H.,

2013. J. Phys. Chem. C 117, 9826-9834.

Galus, Z., 1976, Fundamentals of Electrochemical Analysis, 2nd ed. Ellis Horwood, New York.

Gao, P., Gong, Y.X., Mellott, N.P., Liu, D.W., 2015. Electrochim. Acta 173, 31-39.

Han, M., Guo, P., Wang, X.H., Tu, W.W., Bao, J.C., Hui, D.Z., 2013. RSC Adv. 3, 20456-20463.

Henstridge, M.C., Dickinson, E.J.F., Aslanoglu, M., Batchelor-McAuley, C., Compton, R.G. 2010. Sens. Actuators B 145, 417-427.

Hu, J.J., Wong., N.K., Ye, S., Chen, X.M., Lu, M.Y., Zhao, A.Q., Guo, Y.H., Ma, A.C.H., Leung, A.Y.H., Shen, J.G., Yang, D., 2015. J. Am. Chem. Soc. 137, 6837-6843.

Hyland, K., Auclair, C., 1981. Biochem. Bioph. Res. Co. 102, 531-537.

Jia, L.C., Lawrence, G., Balasubramanian, V.V., Choi, G., Choy, J.H., Abdullah, A.M., Elzatahry, A., Ariga, K., Vinu, A., 2015. Chem. Eur. J. 21, 697-703.

Jia, N.Q., Wen, Y.L., Yang, G.F., Lian, Q., Xu, C.J., Shen, H.B., 2008. Electrochem. Commun. 10,774-777.

Kamin, R.A., Wilson, G.S., 1980. Anal. Chem. 52, 1198-1205.

Kuai, L., Geng, B.Y., Wang, S.Z., Sang, Y., 2012. Chem. Eur. J. 18, 9423-9429.

Kuila, T., Bose, S., Khanra, P., Mishra, A.K., Kim, N.H., Lee, J.H., 2011.

Biosens. Bioelectron. 26, 4637-4648.

Li, S.S., Lv, J.J., Hu, Y.Y., Zheng, J.N., Chen, J.R., Wang, A.J., Feng, J.J., 2014. J. Power Sources 247, 213-218.

Lin, Q.Y., Jin, L.J., Cao, Z.H., Lu, Y.N., Xue, H.Y., Xu, Y.P., 2008. Phytother. Res. 22, 740-745.

Lu, X.B., Zhang, H.J., Ni,Y.W., Zhang, Q., Chen. J.P., 2008. Biosens. Bioelectron. 24, 93-98.

Luo, Y.P., Hu, G.Q., Zhu, A.W., Kong, B., Wang, Z., Liu, C.Y., Tian, Y., 2011. Biosens. Bioelectron. 29, 189-194.

Madhurantakam, S., Selvaraj, S., Nesakumar, N., Sethuraman, S., Rayappan, J.B.B., Krishnan, U.M., 2014. Biosens. Bioelectron. 59, 134-139.

Meany, D.L., Thompson, L., Arriaga, E.A., 2007. Anal. Chem. 79, 4588-4594.

Niu, X.H., Lan, M.B., Zhao, H.L., Chen, C., 2013a. Anal Chem. 85, 3561-3569.

Niu, X.H., Li, Y.X., Tang, J., Hu, Y.L., Zhao, H.L., Lan, M.B., 2014. Biosens. Bioelectron. 51, 22-28.

Niu, X.H., Zhao, H.L., Chen, C., Lan, M.B., 2013b. ChemCatChem 5, 1416-1425.

Ohsaka, T., Tian, Y., Shiod, M., Kasahara, S., Okajima, T., 2002. Chem. Commun. 990-991.

Plowman, B.J., Jones, L.A., Bhargava, S.K., 2015. Chem. Commun. 51, 4331-4346.

Ren, L.X., Dong, J.P., Cheng, X.W., Xu, J.Q., Hu, P.F., 2013. Microchim. Acta180, 1333-1340.

Robinson, K.M., Janes, M.S., Pehar, M., Monette, J.S., Ross, M.F., Hagen, T.M., Murphy, M.P., Beckman, J.S., 2006. Proc. Natl. Acad. Sci. U S A. 103, 15038-15043.

Santhosh, P., Manesh, K.M., Lee, S.H., Uthayakumar, S., Gopalan, A.I., Lee, K.P., 2011. Analyst 136, 1557-1561.

Singh, J., Roychoudhury, A., Srivastava, M., Solanki, P.R., Lee, D.W., Lee, S.H., Malhotra, B.D., 2014. Nanoscale, 6, 1195-1208.

Singh, J., Roychoudhury, A., Srivastava, M., Solanki, P.R., Lee, D.W., Lee, S.H., Malhotra, B.D., 2014. Nanoscale 6, 1195-1208.

Sun, X.L., Guo, S.J., Liu, Y., Sun, S.H., 2012. Nano Lett. 12, 4859-4863.

Tang, J., Zhu, X., Niu, X.H., Liu, T.T., Zhao, H.L., Lan, M.B., 2015. Talanta 137, 18-24.

Trifonov, A., Herkendell, K., Tel-Vered, R., Yehezkeli, O., Woerner, M., Willner, I., 2013. ACS Nano 7, 11358-11368.

Valko, M., Leibfritz, D., Moncol, J., Cronin, M.T., Mazur, M., Telser, J., 2007. Int. J. Biochem. Cell Biol. 39, 44-84.

Wang, D.B., Zhao, L.X., Guo, L.H., Zhang, H., 2014. Anal. Chem. 86, 10535-10539.

Wang, X.H., Han, M., Bao, J.C., Tu, W.W., Dai, Z.H., 2012. Anal. Chim. Acta 717, 61-66.

Wang, Z., Liu, D., Gu, H., Zhu, A.W., Tian, Y., Shi, G.Y., 2013. Biosens. Bioelectron. 43, 101-107.

Wardman, P., 2007. Free Radical Bio. Med. 43, 995-1022.

Wu, H.X., Suzuki, T., Carey, B., Trapnell, B.C., McCormack, F.X., 2011. J. Biol. Chem. 286, 14932-14940.

Yu, J.J., Tu, J.X., Zhao, F.Q., Zeng, B.Z., 2010. J. Solid State Electrochem.14, 1595-1600.

Yuan, L., Liu, S.L., Tu, W.W., Zhang, Z.S., Bao, J.C., Dai, Z.H., 2014. Anal. Chem. 86, 4783-4790.

Zhang, G.R., Wu, J., Xu, B.Q., 2012. J. Phys. Chem. C 116, 20839-20847.

Zheng, Y.N., Chai, Y.Q., Yuan, Y.L., Yuan, R., 2014. Anal. Chim. Acta 834, 45-50.

Zhu, X., Niu, X.H., Zhao, H., Tang, J., Lan, M.B., 2015. Biosens. Bioelectron. 67, 79-85.

Figure captions

Fig. 1. XRD pattern (A), SEM image (B), XPS (C) and EDS pattern (D) of porous Pt-Pd nanomaterial.

Fig. 2. (A) CV curves in 0.1 M H_2SO_4 at scan rate of 50 mV s^{-1} (B) the EIS curves in 100 mM KCl solution containing 5 mM $Fe(CN)_6^{3-/4-}$ with the frequency ranging from 100 kHz to 0.01 Hz for SOD/SPCE, SOD/dense Pt-Pd/SPCE and SOD/porous Pt-Pd/SPCE.

Fig. 3. CV curves of the (A) SOD/dense Pt-Pd/SPCE and SOD/porous Pt-Pd/SPCE (B) in 0.05 M PBS (pH 7.4) with the absence and presence of different amounts of KO_2 (different concentrations of $O_2^{\bullet-}$) at scan rate of 20 mV s^{-1}. The right figures represent the enlarged drawings of reduction peaks.

Fig. 4. Amperometric response of the SOD/porous Pt-Pd/SPCE for the successive addition of $O_2^{\bullet-}$ into constantly stirred 0.05 M PBS (pH 7.4). Applied potential: -0.1 V. Inset is the relationship between amperometric responses and $O_2^{\bullet-}$ concentration (n = 5).

Fig. 5 Amperometric responses toward $O_2^{\bullet-}$ released from HeLa cells. Curve a: addition of 20 μL Zymosan A (5 mg/mL) to PBS (pH = 7.4) without Hela cells; Curve b: addition of 20 μL PBS to Hela cells suspension; Curve c: addition of 20 μL Zymosan A to Hela cells suspension.

Table 1. Comparison of the analytical performance of various electrodes for $O_2^{\bullet-}$ sensing.

Electrode	Applied potential (V)	Sensitivity ($\mu A\ cm^{-2}\ mM^{-1}$)	LOD (μM)	Linear range (μM)	Ref.
SOD/SA	0	0.782	0.23	0.4-229.9	(Wang et al. 2012)
SOD/Pt-Pd/MWCNTs/SPGE	-0.1	601	0.71	40-1,550	(Zhu et al. 2015)
SOD/PtPd-PDARGO	-0.3	909.7	2	16-240	(Tang et al. 2015)
PMMA/PANI-Au-nano/SOD-ESCFM	0.3	42.5	0.3	0.5-2.4	(Santhosh et al. 2011)
SOD/mesoporous SiO_2–(L)-lysine	0.05	91.2	0.8	3.11–176.53	(Han et al. 2013)
SOD/GC/NTA	0.2	264	0.021	0.1-100	(Wang et al. 2013)
SOD/Gelatin	0.65	43.01	10	20-2000	(Emregül 2005)
SOD/ZnO	0	17.1	0.1	0.12-250	(Deng et al. 2008a)
SOD/Au NP	0.25	24.5	0.1	0.2-220	(Santhosh et al. 2011)
SOD/porous Pt-Pd/SPCE	**-0.1**	**1270**	**0.13**	**16-1536**	**This work**

SOD: Superoxide Dismutase; SA: Sodium alginate; SPGE: Screen printed gold electrode; PDARGO: Chemically reduced graphene oxide coated with polydopamine; PMMA: Poly(methyl-methacrylate); PANI: Polyaniline; ESCFM: Electrospun nanofibers; CS, Cys: Cysteine; NTA: Nitrilotriacetic acid.

Highlights

- A captivating porous Pt-Pd interface for the immobilization of SOD
- Ultrahigh sensitive and selective sensing of $O_2^{\bullet-}$;
- Capturing the trace level of $O_2^{\bullet-}$ released from stimulated cells.

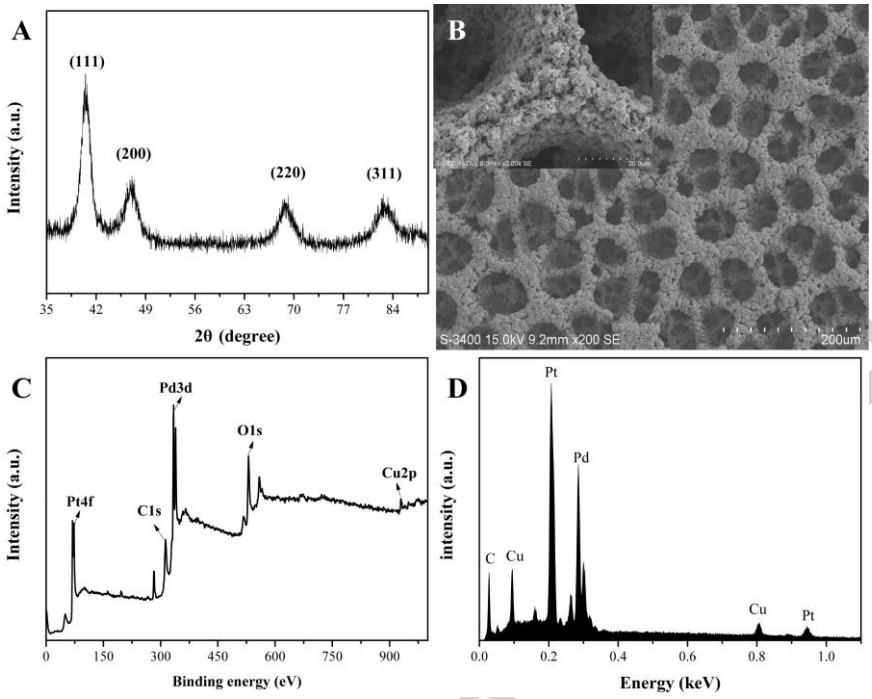

fig 1

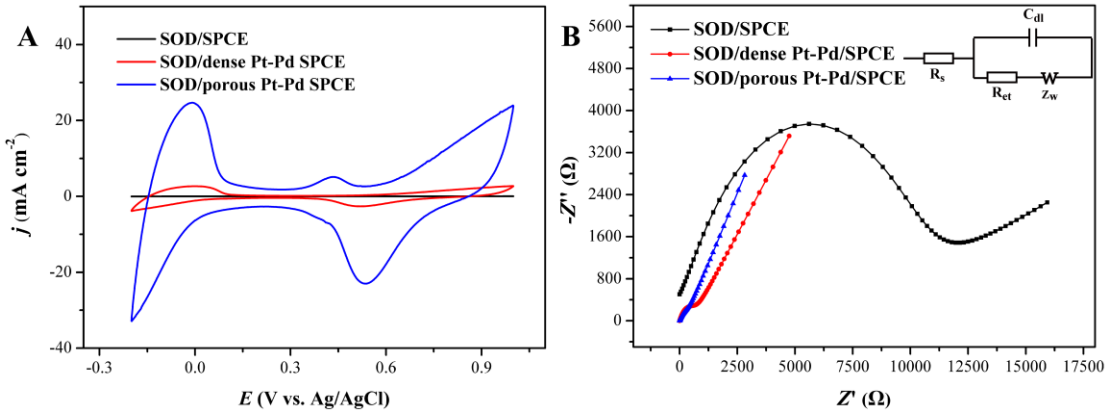

fig 2

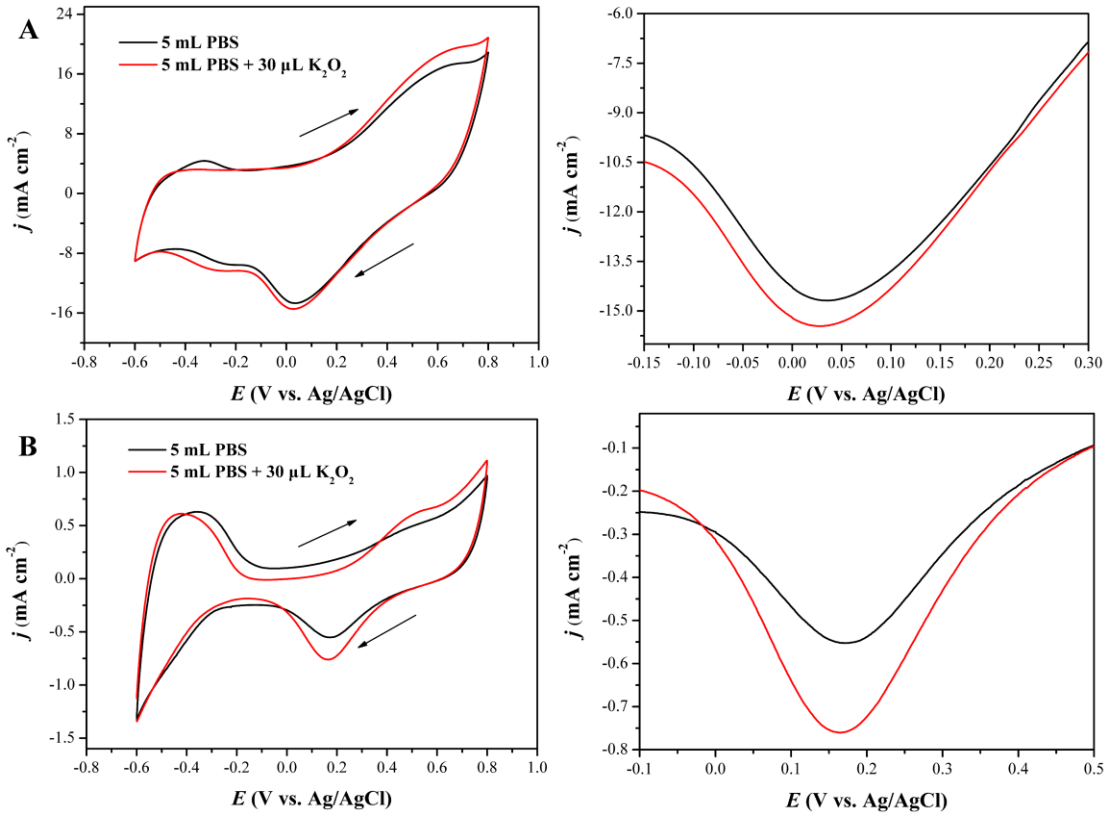
A
5 mL PBS
5 mL PBS + 30 µL K_2O_2
j (mA cm^{-2})
E (V vs. Ag/AgCl)
B
5 mL PBS
5 mL PBS + 30 µL K_2O_2
j (mA cm^{-2})
E (V vs. Ag/AgCl)

fig 3

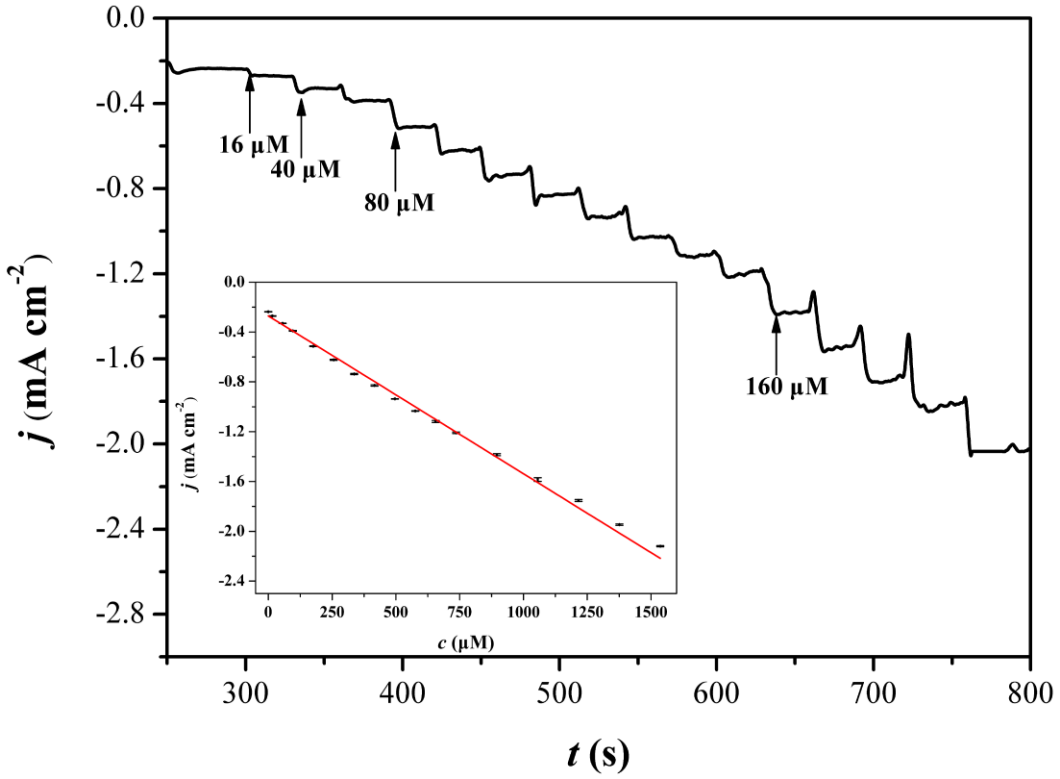
16 µM
40 µM
80 µM
160 µM
j (mA cm^{-2})
t (s)
c (µM)

fig 4

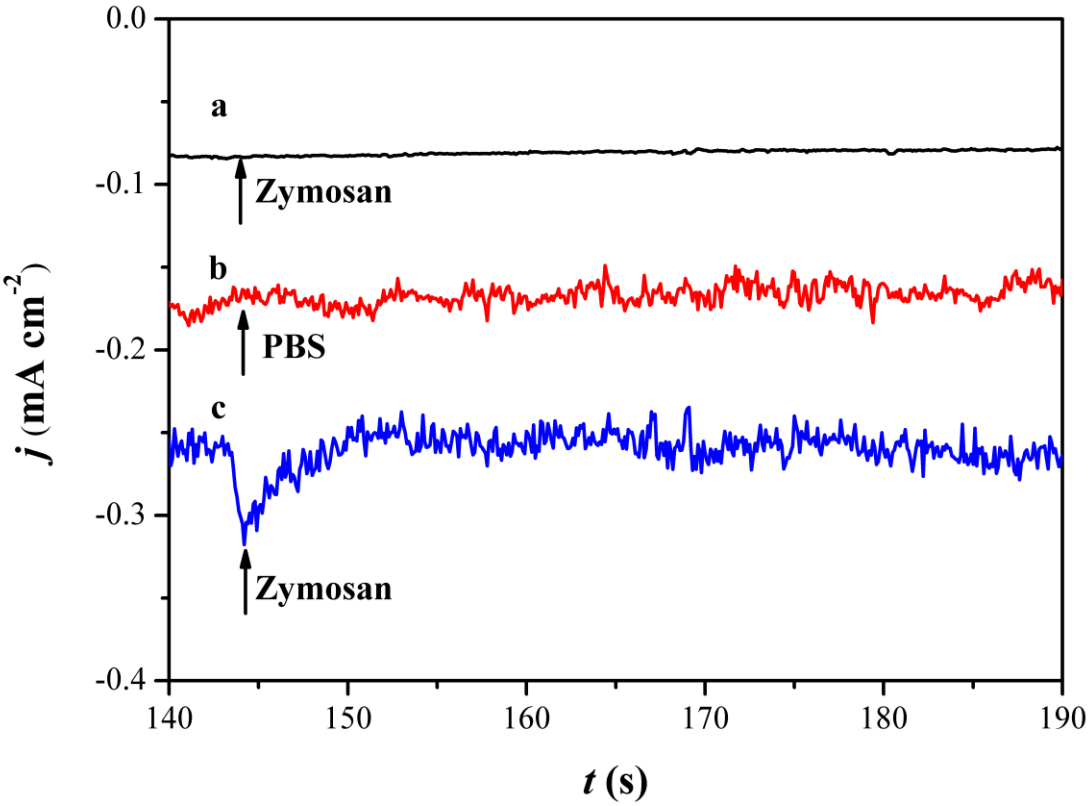

fig 5